infall is balanced by outward radiation pressure. Consequently, the kinetic power of the wind is $P_{kin} \sim 2 \times 10^{46}$ erg/s, or 20% of the bolometric luminosity of the quasar. According to models and simulations (*19*, *20*), the deposition of a few percent of the total radiated energy is sufficient to prompt an appreciable feedback on the host galaxy. Because most of the kinetic output will be ultimately transferred to the surrounding gas (*21*), these conditions are met even if R_{in} is set to the escape radius (~30 r_g for v_{out} = 0.25 c), the minimum plausible starting point of the wind.

The mechanical energy released over a period of 10^7 years (i.e., one-tenth of a typical quasar lifetime) is close to 10^{61} erg, comparable to or exceeding the expected binding energy of the galactic bulge in a system like PDS 456. The large opening angle evinced here suggests that the coupling of the outflow with the gas in the host galaxy will be effective, as required for strong negative feedback. We are then possibly witnessing the initial stage of the sweeping process that leads to molecular mass losses of hundreds to thousands M_{Sun}/year even in sources with no powerful radio jets (*22*). For a commensurate kinetic luminosity, in fact, the observed galaxy-wide outflows entail considerable mass loading and momentum boost.

A fundamental correlation (the so-called $M-\sigma_*$ scaling relation) exists between the mass of the central black holes and the stellar velocity dispersion of galactic bulges on kpc scales (*23*, *24*)—that is, hundreds of times beyond the gravitational sphere of influence of the black holes themselves. It is still debated whether this is the product of a feedback-driven black hole/host galaxy coevolution (*25*) or of a hierarchical assembly through galaxy mergers (*26*). Identifying wide-angle accretion disk winds in the Eddington-limited regime lends weight to the idea that AGN have a substantial impact on the surrounding environment. As a rare, nearby analog of the luminous AGN population at high redshift, PDS 456 shows a flavor of cosmic feedback, believed to have operated at the peak of the quasar epoch about 10 billion years ago. In distant galaxies in a similar activity phase, such powerful winds would have provided the energy and momentum to self-regulate the black hole growth and control the star formation in stellar bulges, leaving the present-day scaling relations as a record of this process (*27*).

REFERENCES AND NOTES

1. A. R. King, *Mon. Not. R. Astron. Soc.* **402**, 1516–1522 (2010).
2. F. Tombesi *et al.*, *Astron. Astrophys.* **521**, A57 (2010).
3. J. Gofford *et al.*, *Mon. Not. R. Astron. Soc.* **430**, 60–80 (2013).
4. J. Silk, M. J. Rees, *Astron. Astrophys.* **331**, L1 (1998).
5. J. Kormendy, L. C. Ho, *Annu. Rev. Astron. Astrophys.* **51**, 511–653 (2013).
6. J. N. Reeves, P. T. O'Brien, M. J. Ward, *Astrophys. J.* **593**, L65–L68 (2003).
7. J. N. Reeves *et al.*, *Astrophys. J.* **701**, 493–507 (2009).
8. J. N. Reeves *et al.*, *Astrophys. J.* **780**, 45 (2014).
9. Materials and methods are available as supplementary materials on *Science* Online.
10. C. Done, M. A. Sobolewska, M. Gierliński, N. J. Schurch, *Mon. Not. R. Astron. Soc.* **374**, L15–L19 (2007).
11. J. S. Kaastra *et al.*, *Science* **345**, 64–68 (2014).
12. L. C. Gallo, A. C. Fabian, *Mon. Not. R. Astron. Soc.* **434**, L66–L69 (2013).
13. K. A. Pounds, J. N. Reeves, *Mon. Not. R. Astron. Soc.* **397**, 249–257 (2009).
14. N. Arav, B. Borguet, C. Chamberlain, D. Edmonds, C. Danforth, *Mon. Not. R. Astron. Soc.* **436**, 3286–3305 (2013).
15. Y. Krongold *et al.*, *Astrophys. J.* **659**, 1022–1039 (2007).
16. F. Tombesi, M. Cappi, J. N. Reeves, V. Braito, *Mon. Not. R. Astron. Soc.* **422**, L1–L5 (2012).
17. D. Proga, J. M. Stone, T. R. Kallman, *Astrophys. J.* **543**, 686–696 (2000).
18. J. Gofford *et al.*, *Astrophys. J.* **784**, 77 (2014).
19. T. Di Matteo, V. Springel, L. Hernquist, *Nature* **433**, 604–607 (2005).
20. P. F. Hopkins, M. Elvis, *Mon. Not. R. Astron. Soc.* **401**, 7–14 (2010).
21. K. Zubovas, A. King, *Astrophys. J.* **745**, L34 (2012).
22. C. Cicone *et al.*, *Astron. Astrophys.* **562**, A21 (2014).
23. L. Ferrarese, D. Merritt, *Astrophys. J.* **539**, L9–L12 (2000).
24. K. Gebhardt *et al.*, *Astrophys. J.* **539**, L13–L16 (2000).
25. A. R. King, *Astrophys. J.* **596**, L27–L29 (2003).
26. K. Jahnke, A. V. Macciò, *Astrophys. J.* **734**, 92 (2011).
27. R. C. McQuillin, D. E. McLaughlin, *Mon. Not. R. Astron. Soc.* **434**, 1332–1338 (2013).

ACKNOWLEDGMENTS

This research was supported under the U.K. Science and Technology Facilities Council grant ST/J001384/1 and is based on x-ray observations obtained with the XMM-Newton and NuSTAR satellites. XMM-Newton is a European Space Agency (ESA) science mission with instruments and contributions directly funded by ESA member states and the National Aeronautics and Space Administration. The NuSTAR mission is a project led by the California Institute of Technology, managed by the Jet Propulsion Laboratory, and funded by NASA. We thank the NuSTAR Operations, Software, and Calibration teams for support with execution and analysis of these observations. We also acknowledge financial support from the Italian Space Agency under grant ASI-INAF I/037/12/0 (G.R. and G.M.); the Italian National Institute for Astrophysics under grant PRIN-INAF 2012 (G.R.); the I-CORE program of the Planning and Budgeting Committee, the Israel Science Foundation under grants 1937/12 and 1163/10, Israel's Ministry of Science and Technology (E.B.); and NASA under grants NNX11AJ57G and NNG08FD60C (T.J.T.). The data are stored in the science archives of the two x-ray observatories involved and will become publicly available on 25 March 2015 (XMM-Newton) and with the upcoming DR6 data release (NuSTAR).

SUPPLEMENTARY MATERIALS

www.sciencemag.org/content/347/6224/860/suppl/DC1
Materials and Methods
Supplementary Text
Figs. S1 to S5
Tables S1 to S3
References (*28*–*63*)

25 July 2014; accepted 20 January 2015
10.1126/science.1259202

TRANSITION STATES

Trapping a transition state in a computationally designed protein bottle

Aaron D. Pearson,[1]* Jeremy H. Mills,[2]* Yifan Song,[2] Fariborz Nasertorabi,[3] Gye Won Han,[3] David Baker,[2,4] Raymond C. Stevens,[3] Peter G. Schultz[1]†

The fleeting lifetimes of the transition states (TSs) of chemical reactions make determination of their three-dimensional structures by diffraction methods a challenge. Here, we used packing interactions within the core of a protein to stabilize the planar TS conformation for rotation around the central carbon-carbon bond of biphenyl so that it could be directly observed by x-ray crystallography. The computational protein design software Rosetta was used to design a pocket within threonyl-transfer RNA synthetase from the thermophile *Pyrococcus abyssi* that forms complementary van der Waals interactions with a planar biphenyl. This latter moiety was introduced biosynthetically as the side chain of the noncanonical amino acid *p*-biphenylalanine. Through iterative rounds of computational design and structural analysis, we identified a protein in which the side chain of *p*-biphenylalanine is trapped in the energetically disfavored, coplanar conformation of the TS of the bond rotation reaction.

The direct observation of the transition state (TS) of a chemical reaction requires highly sensitive spectroscopic techniques with a temporal resolution on the order of 10^{-13} to 10^{-14} s. This milestone was made possible with the advent of ultrafast laser spectroscopy, which allowed the direct observation of the transient species formed as reactants cross an energy barrier to products (*1*, *2*). However, determination of the three-dimensional (3D) structure of a TS requires ultrafast electron or x-ray diffraction techniques with similar temporal resolution and sensitivity (*3*, *4*). An alternative approach is to increase the lifetime of the transition state configuration by trapping it in a free energy (ΔG) well so that it can be directly observed by more conventional spectroscopic methods. In theory, the well-packed interior of a protein could act as a "programmable" solvent to selectively stabilize a TS configuration and thereby make it kinetically persistent and directly observable by conventional x-ray diffraction methods. Indeed, enzymes

[1]Department of Chemistry and Skaggs Institute for Chemical Biology, The Scripps Research Institute, La Jolla, CA 92037, USA. [2]Department of Biochemistry, University of Washington, Seattle, WA 98195, USA. [3]Department of Biological Sciences, Bridge Institute, University of Southern California, Los Angeles, CA 90089, USA. [4]Howard Hughes Medical Institute (HHMI), University of Washington, Seattle, WA 98195, USA.
*These authors contributed equally to this work. †Corresponding author. E-mail: schultz@scripps.edu

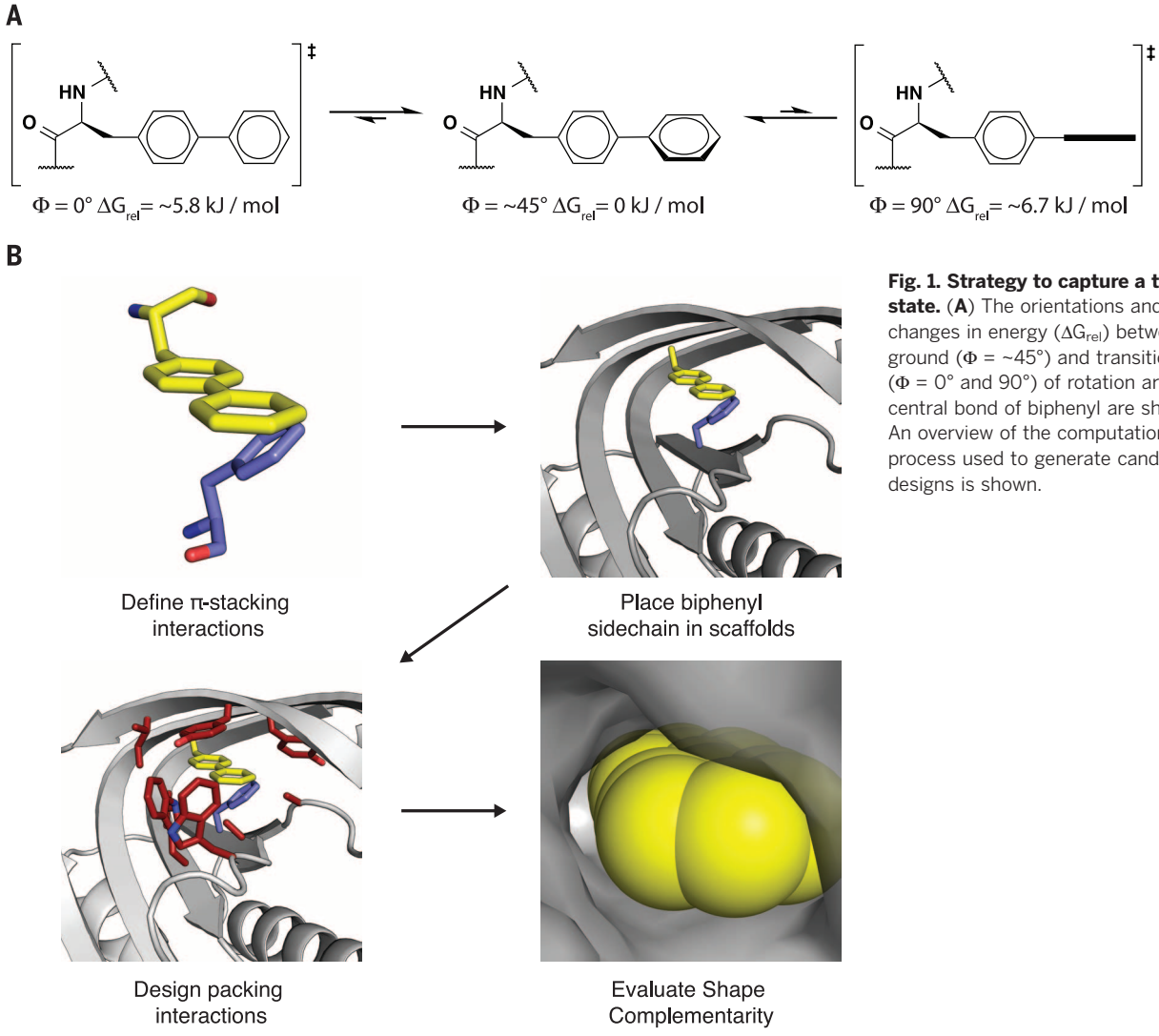

Fig. 1. Strategy to capture a transition state. (**A**) The orientations and relative changes in energy (ΔG_{rel}) between the ground (Φ = ~45°) and transition states (Φ = 0° and 90°) of rotation around the central bond of biphenyl are shown. (**B**) An overview of the computational design process used to generate candidate designs is shown.

catalyze reactions by virtue of their ability to selectively stabilize the rate-limiting TS relative to the ground-state reactants (*5*–*9*). Here, we show the redesign of the interior of the protein threonyl-tRNA synthetase from the thermophile *Pyrococcus abyssi* (*10*) to create a microenvironment that has high complementarity to the planar TS configuration for rotation about the central C–C bond of biphenyl (*11*). Determination of the 3D structure of the designed protein at 2.05 Å resolution by x-ray crystallography revealed a planar biphenyl TS configuration stabilized by van der Waals interactions with side chains in the protein core.

Biphenyl bond rotation is a well-studied reaction, both experimentally and theoretically. In the gas phase, the ground state of biphenyl is twisted, with a dihedral angle of ~45°. Rotation around the central C–C bond connecting the two phenyl rings in biphenyl is estimated to have an energy barrier of 5.8 ± 2.1 and 6.7 ± 2.1 kJ/mol around the 0° (planar) and 90° TSs, respectively, as determined experimentally by electron diffraction studies (Fig. 1A) (*12*). The energy barriers estimated using Raman data (*13*, *14*) and ultraviolet absorption spectroscopy (*15*) are in general agreement with the results from the diffraction studies. Theoretical calculations show that these barriers result from opposing steric and electronic effects of the two phenyl rings but give a range of values depending on the method used (*16*). This simple reaction (which racemizes chiral biphenyls) provides an ideal system to pose the question whether side chain packing interactions in a folded protein can be exploited to make a transition state configuration kinetically persistent so that it can be directly observed by x-ray crystallography.

Table 1. First-round computational designs. Designed protein names, parent scaffolds, and mutations made are listed. Single-letter abbreviations for the amino acid residues are as follows: A, Ala; C, Cys; D, Asp; E, Glu; F, Phe; G, Gly; H, His; I, Ile; K, Lys; L, Leu; M, Met; N, Asn; P, Pro; Q, Gln; R, Arg; S, Ser; T, Thr; V, Val; W, Trp; and Y, Tyr.

Designed protein	Parent scaffold (PDB ID)	Computationally designed mutations
BIF_1	1y2q	$S^{8}A$, I^{11}BiPhe, $F^{42}W$, $Y^{79}A$, $F^{81}W$, $K^{121}I$, $F^{123}Y$
BIF_2	1anu	$V^{20}G$, $F^{22}I$, $C^{33}W$, F^{35}BiPhe, $F^{37}W$, $F^{96}G$
BIF_3	2h2h	$F^{48}L$, F^{60}BiPhe, $Y^{61}W$, $F^{63}W$, $A^{64}M$, $I^{68}G$, $P^{157}G$, $I^{159}A$
BIF_4	1ve0	$I^{21}T$, V^{25}BiPhe, $S^{26}A$, $V^{39}G$, $C^{46}A$, $I^{48}V$

To introduce a biphenyl moiety into a protein core, we used the genetically encoded noncanonical amino acid *p*-biphenylalanine (BiPhe). This amino acid can be introduced site-specifically into a protein in *Escherichia coli* in good yield in response to the amber nonsense codon TAG, with an orthogonal amber suppressor tRNA/aminoacyl-tRNA synthetase (aaRS) pair. The aaRS was evolved from the *Methanococcus jannaschi* tyrosyl-tRNA synthetase to be selective for BiPhe and not incorporate any of the 20 canonical amino acids (*17*, *18*). The rotational barrier around

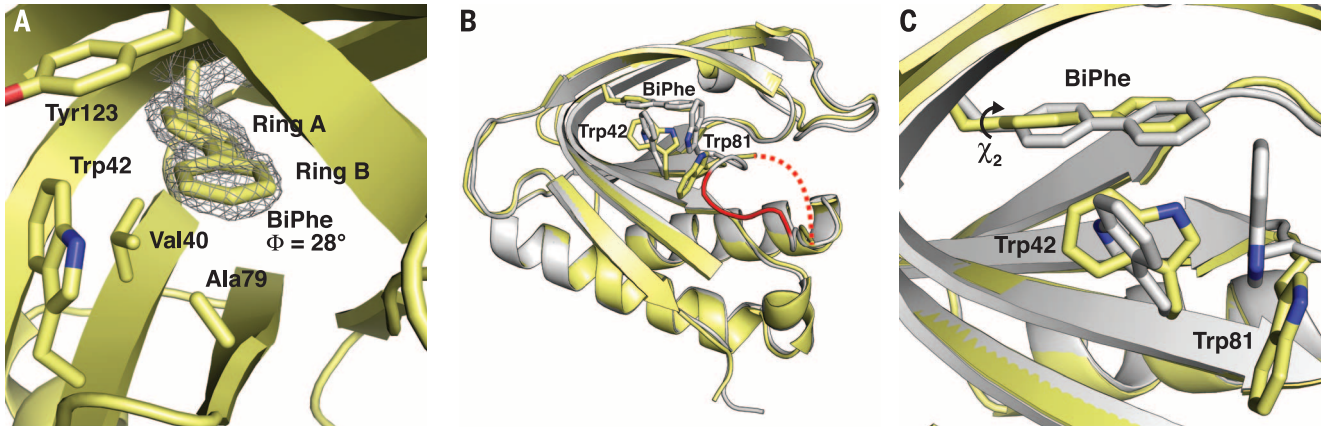

Fig. 2. X-ray crystallographic analysis of BIF_1. (**A**) The x-ray crystal structure of BIF_1 is shown in yellow; BiPhe and surrounding residues are shown in sticks. Rings A and B are those closest to and farthest from the protein backbone, respectively. Electron density around the BiPhe side chain is shown as a $2F_o - F_c$ map contoured to 2σ. (**B**) A comparison of the design model (gray) to the structure (yellow) of BIF_1 is shown; BiPhe, Trp^{42}, and Trp^{81} are shown in sticks. A loop corresponding to residues 81 to 89 of the parent scaffold is shown in red. Missing density in the structure corresponding to residues 83 to 86 of BIF_1 is shown as a dashed red line. (**C**) A comparison of the structure of BIF_1 (yellow) to the design model (gray) is shown. BiPhe, Trp^{42}, and Trp^{81} are shown in sticks. An arrow indicates rotation about χ^2 in the structure relative to the design.

Table 2. Second- and third-round crystallographic analysis. Second-round mutant identities, biphenylalanine dihedral angle, and x-ray crystal structure resolution are listed. Dihedrals listed are averages of those measured on each side of the biphenyl ring.

Scaffold	F^{42}	Y^{79}	F^{123}	BIF Φ (deg.)	Resolution (Å)
BIF_1	W	A	Y	26	1.95
BIF_1.1	F	S	V	35	2.10
BIF_1.2	F	V	V	21	2.50
BIF_1.3	F	S	A	15	2.36
BIF_1.4	F	V	A	20	2.10
BIF_0	F	I	A	0	2.05

the biphenyl C–C bond in BiPhe is not expected to be substantially different from biphenyl itself (*19*).

To identify an appropriate host protein in which to construct a site complementary to the planar biphenyl TS geometry, we first curated a set of ~2300 proteins of known structures from thermophilic organisms [a full description of the computational design process is found in the supplementary materials (*20*)]. Proteins with high thermostabilities have more negative Δ*G*s of folding and are in general more tolerant to mutations; both characteristics are likely to be beneficial when attempting to stabilize a TS configuration through packing interactions in a protein core (*21*, *22*). RosettaMatch (*23*) was then used to identify residues in the core of each protein scaffold where BiPhe could be substituted without creating unfavorable steric interactions with the protein backbone (Fig. 1B), and make π-stacking interactions (*24*) with native Trp, Phe, or Tyr residues. Because the RosettaMatch calculations were carried out with a planar model of the BiPhe, these interactions should stabilize the biphenyl side chain in the desired planar TS conformation. To ensure that the substituted BiPhe side chain was sufficiently buried within a particular protein's core, initial hits were first filtered on the basis of the change in solvent-accessible surface area (ΔSASA) (*25*) that occurs when BiPhe is removed from the substituted site. A ΔSASA cutoff of 0.9 (meaning the BiPhe was >90% buried) removed 35% of the initial matches from further consideration.

RosettaDesign (*26*) was then used to optimize the identities of residues surrounding the BiPhe (excluding residues already participating in π-stacking interactions) such that they packed tightly against the planar BiPhe side chain but did not create unfavorable hydrogen-bonding interactions (Fig. 1B). Candidate designs were ranked by shape complementarity (SC) (*27*) between the designed residues and the BiPhe (Fig. 1B). Ultimately, four designs (BIF_1 to BIF_4) with high SC values were chosen for experimental characterization (Table 1). The computer-modeled proteins containing the BiPhe were reverse-translated and optimized for expression in *E. coli*.

To incorporate BiPhe into these four different protein scaffolds, we used the orthogonal amber suppressor tRNA/BiPheRS pair encoded on the dual-plasmid expression system (pUltra) (*28*). One plasmid contained the tRNA/BiPheRS pair specific for BiPhe, and the other contained the synthetic mutant gene of interest fused to a C-terminal hexa-histidine purification tag. A TAG amber nonsense codon was introduced at the desired site to encode BiPhe (*17*). These plasmids were cotransformed into *E. coli* Bl21(DE3), and protein expression was carried out in the presence of 1 mM BiPhe. Proteins were purified from cell lysate via Ni^{2+}-affinity chromatography followed by size-exclusion chromatography. Mass spectrometric analysis of BIF_1 to BIF_4 indicated successful incorporation of BiPhe in all cases (fig. S1), and SDS–polyacrylamide gel electrophoresis indicated that the purified proteins were of suitable purity (>95%) for crystallographic analysis.

All four designed proteins were subjected to an initial crystallographic screen based on the conditions used to crystallize the wild-type protein (*20*, *29*–*32*). Crystals were obtained only for BIF_1, which has as its parent scaffold threonyl-tRNA synthetase from the thermophile P. *abyssi*, but they were needles and not suitable for x-ray crystallography. An automated high-throughput crystallization system was then used to identify new conditions (0.1 M sodium citrate, 15% polyethylene glycol 6000, pH = 5.5) in which large crystals of BIF_1 grew. The structure of BIF_1 was solved to 1.8 Å resolution by x-ray crystallography using molecular replacement with the parent scaffold (PDB ID 1y2q) serving as a search model. Density for BiPhe was clearly observed in a $2F_o - F_c$ map (Fig. 2A), and the torsion angle between the two phenyl rings was determined to be ~28° (Fig. 2A). This value represented a rotation of ~17° toward the desired planar conformation relative to the dihedral found at the energetic minimum but remained far from the desired value of 0°. To force the BiPhe torsion angle closer to planarity, a second round of computational design was undertaken on the basis of a detailed analysis of the structure of BIF_1.

Globally, the structure of BIF_1 matched the design model quite well (Fig. 2B; root mean square deviation to the design model of ~1.3 Å over all atoms), although differences are apparent in the vicinity of the BiPhe residue. In the model, Trp^{42} and Trp^{81} both form edgewise interactions with the BiPhe side chain. However, in the crystal

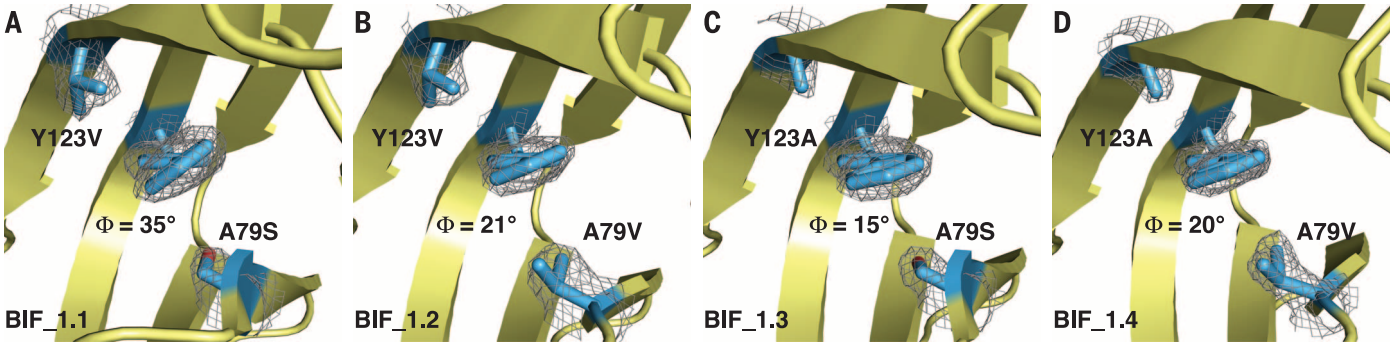

Fig. 3. A comparison of the crystal structures of BIF_1.1 to BIF_1.4. (**A** to **D**) Crystal structures of second-round mutants BIF_1.1 to BIF_1.4 are shown. The side chains of BiPhe, and those at positions 79 and 123, are shown in sticks. Electron density from a $2F_o - F_c$ map contoured to 1.5σ [(A to C)] and 2.0σ (D) is shown for the aforementioned residues. The measured dihedral angle between the two biphenyl rings is shown beneath the biphenyl side chain in each case.

structure, the indole ring of Trp[42] rotates such that it packs lengthwise against the BiPhe side chain in an orientation that would clash with the side-chain orientation of Trp[81] predicted by the design model (Fig. 2C). To avoid this unfavorable steric interaction, a substantial displacement of the loop consisting of residues 81 to 89 likely occurs, as evidenced by the lack of electron density for residues 83 to 86 in the crystal structure (Fig. 2B). In an attempt to return the disordered loop to its native position, we independently mutated each Trp to Phe (the wild-type residue at both positions) in silico. Unconstrained repacking and minimization calculations in the context of each mutation showed that Trp[42]Phe increased SC and scored slightly better than the original design. As a result, this mutation was made standard for the remainder of the computational redesign.

A second focus of the redesign effort was to identify point mutations in residues packing against the biphenyl rings to force the side chain into the desired planar conformation. In the structure of BIF_1, the biphenyl side chain is rotated ~5° about χ_1 and 25° about χ_2, relative to its placement in the design model (Fig. 2C). Although the phenyl ring closest to the backbone (ring A) is out of plane with respect to the model, the ring farthest from the backbone (ring B) is essentially in the plane of the design model (Fig. 2, A and C). Thus, it appears that rotation about χ_2 is the predominant determinant of the 28° deviation from planarity observed in the crystal structure relative to the design model. Because ring A is bounded on one face by the protein backbone, we believed it would be difficult to identify a mutant that would adjust this ring in the desired direction (Fig. 2C). In contrast, ring B is flanked by both Ala[79] and Tyr[123], suggesting that mutagenesis of one or both of these residues could potentially planarize the BiPhe dihedral angle (Fig. 2A). Analysis of the structure of BIF_1 suggested that the phenyl ring of Tyr[123] likely prevents ring B from rotating into the plane of ring A (Fig. 2A); thus, we mutated Tyr[123] in silico to the smaller residues Ala and Val. Concurrently, Ala[79] was mutated to the bulkier residues Cys, Ser, Thr, and Val. Rosetta was then used to analyze these potential sequence alternatives, again by carrying out unconstrained repacking and minimization calculations. The energies for all mutants tested fell within ~6 Rosetta energy units (REU) of one another and gave SC values that differed at most by ~5%. The tight distribution of values for both metrics suggested that no clear preference exists for one mutant over another, so a series of four mutants was examined experimentally.

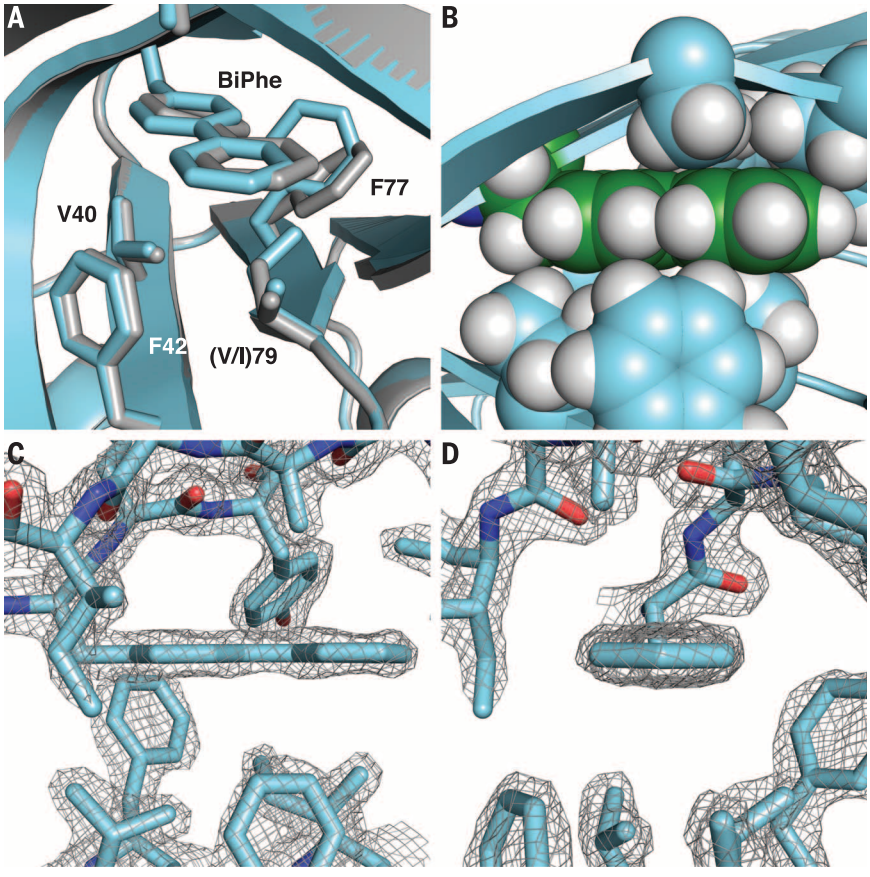

Fig. 4. X-ray crystal structure of BIF_0. (**A**) The crystal structure of BIF_0 is shown in blue, and BIF_1.3 is shown in gray. The BiPhe side chain and surrounding residues are shown in sticks. (**B**) Packing interactions between the designed protein BIF_0 and the BiPhe side are highlighted with space-filling representations of the interacting residues. (**C** and **D**) The structure of BIF_0 is shown, highlighting the BiPhe side chain; views from the front and side are shown. The BiPhe side chain and surrounding residues are shown in sticks, and $2F_o - F_c$ maps are contoured to 2σ in each case.

All four mutants expressed well and afforded diffraction-quality crystals. We solved the structures of BIF_1.1, BIF_1.2, BIF_ 1.3, and BIF_1.4 to 2.10, 2.50, 2.36, and 2.10 Å resolution, respectively, again by molecular replacement. In all cases, the Trp[42]Phe mutation returned the displaced loop to its native position (fig. S2). However, a distribution of BiPhe torsion angles between 35°

and 15° was observed among the four structures (Table 2). In the majority of these cases, the change in the χ_2 angle relative to the original design remained near the value of 25° observed in the initial BIF_1 structure. This result suggested that mutations to Ala^{79} and Trp^{123} have the desired effect of rotating ring B without affecting the absolute orientation of ring A. Unfortunately, substitution of Tyr^{123} with the beta-branched Val and the opposing Ala^{79} with Ser (BIF_1.1) had the effect of rotating ring B even farther out of plane (35°) than in the original structure (Fig. 3A). This undesired rotation was partially remedied in BIF_1.2 (Φ = 21°) (Fig. 3B) by substituting Ala^{79} with a bulkier Val residue and further corrected in BIF_1.3 and BIF_1.4 (Φ = 15° and 20°, respectively) (Fig. 3, C and D) by replacing the opposing Tyr^{123} with a smaller Ala residue and Ala^{79} with Ser (BIF_1.3) or Val (BIF_1.4). This analysis suggested that ring A could potentially be rotated into a coplanar geometry by further increasing the size of the amino acid at position 79 with an Ala^{79}Ile mutation while maintaining Phe^{42} and the Tyr^{123}Ala mutation. The additional methyl group of the isoleucine should force the side of ring A to rotate further in the desired direction.

We next generated the corresponding BIF_0 mutant (S^8A, I^{11}BiPhe, Y^{79}I, F^{81}W, K^{121}I, and F^{123}A), purified the protein, and solved its crystal structure to 2.05 Å resolution (Fig. 4). Analysis of the electron density showed that the two phenyl rings of BiPhe are coplanar, which matches the configuration of the TS for the bond rotation reaction. The structure of BIF_0 shows that, in addition to adding steric bulk beneath ring A, the V^{79}I mutation also forces the side chain of Phe^{77} to adopt a different rotamer than was observed in BIF_1.4, which has the effect of further rotating ring A into the plane of ring B (Fig. 4). The mutations introduced into BIF_0 do not appear to substantially affect the thermal stability of the protein. The melting temperature of this mutant, as determined by differential scanning calorimetry, was ~110°C, consistent with the 3D structure of BIF_0, which shows that the protein core is well packed.

We have shown by iterative computational design, mutagenesis, and protein structure determination that one can design a protein core that stabilizes a simple conformational transition state to such a degree that one can determine its 3D x-ray crystal structure. However, we should note that the biphenyl energy landscape corresponds to a substructure within the protein relative to the energetics of the global protein conformational ensemble. A similar strategy was recently employed to directly observe catalyst-substrate interactions through x-ray crystallographic analysis (*33*). The results described here may not be all that surprising given that enzymes typically stabilize a rate-limiting TS by 8 to 12 kcal/mol. Nonetheless, these experiments underscore the ability of proteins to fold into defined 3D structures in which van der Waals, hydrogen-bonding, and electrostatic interactions can be controlled with exquisite precision.

REFERENCES AND NOTES

1. T. S. Rose, M. J. Rosker, A. H. Zewail, *J. Chem. Phys.* **88**, 6672–6673 (1988).
2. J. C. Polanyi, A. H. Zewail, *Acc. Chem. Res.* **28**, 119–132 (1995).
3. R. Srinivasan, J. S. Feenstra, S. T. Park, S. Xu, A. H. Zewail, *Science* **307**, 558–563 (2005).
4. H. Ihee *et al.*, *Science* **291**, 458–462 (2001).
5. L. Pauling, *Chem. Eng. News* **24**, 1375–1377 (1946).
6. W. P. Jencks, *Catalysis in Chemistry and Enzymology* (Dover, Mineola, NY, 1987).
7. A. Tramontano, K. D. Janda, R. A. Lerner, *Science* **234**, 1566–1570 (1986).
8. S. J. Pollack, J. W. Jacobs, P. G. Schultz, *Science* **234**, 1570–1573 (1986).
9. P. G. Schultz, R. A. Lerner, *Science* **269**, 1835–1842 (1995).
10. S. Dwivedi, S. P. Kruparani, R. Sankaranarayanan, *Nat. Struct. Mol. Biol.* **12**, 556–557 (2005).
11. F. Ceccacci, G. Mancini, P. Mencarelli, C. Villani, *Tetrahedron Asymmetry* **14**, 3117–3122 (2003).
12. A. Almenningen *et al.*, *J. Mol. Struct.* **128**, 59–76 (1985).
13. J. E. Katon, E. R. Lippincott, *Spectrochimica Acta* **15**, 627–650 (1959).
14. L. A. Carreira, T. G. Towns, *J. Mol. Struct.* **41**, 1–9 (1977).
15. H. Suzuki, *Bull. Chem. Soc. Jpn.* **32**, 1340–1350 (1959).
16. O. Bastiansen, S. Samdal, *J. Mol. Struct.* **128**, 115–125 (1985).
17. J. Xie, W. Liu, P. G. Schultz, *Angew. Chem. Int. Ed.* **46**, 9239–9242 (2007).
18. L. Wang, A. Brock, B. Herberich, P. G. Schultz, *Science* **292**, 498–500 (2001).
19. J. K. Eloranta, *Zeitschrift Naturforschung Teil A* **27a**, 1652–1662 (1972).
20. Materials and methods are available as supplementary materials on *Science* Online.
21. A. Razvi, J. M. Scholtz, *Protein Sci.* **15**, 1569–1578 (2006).
22. J. D. Bloom, S. T. Labthavikul, C. R. Otey, F. H. Arnold, *Proc. Natl. Acad. Sci. U.S.A.* **103**, 5869–5874 (2006).
23. A. Zanghellini *et al.*, *Protein Sci.* **15**, 2785–2794 (2006).
24. G. B. McGaughey, M. Gagné, A. K. Rappé, *J. Biol. Chem.* **273**, 15458–15463 (1998).
25. S. M. Le Grand, K. M. Merz, *J. Comput. Chem.* **14**, 349–352 (1993).
26. B. Kuhlman, D. Baker, *Proc. Natl. Acad. Sci. U.S.A.* **97**, 10383–10388 (2000).
27. M. C. Lawrence, P. M. Colman, *J. Mol. Biol.* **234**, 946–950 (1993).
28. A. Chatterjee, M. J. Lajoie, H. Xiao, G. M. Church, P. G. Schultz, *ChemBioChem* **15**, 1782–1786 (2014).
29. L. J. Shimon *et al.*, *Structure* **5**, 381–390 (1997).
30. S. Dwivedi, S. P. Kruparani, R. Sankaranarayanan, *Acta Crystallogr. D Biol. Crystallogr.* **60**, 1662–1664 (2004).
31. Y. Tanaka *et al.*, *Proteins* **61**, 1127–1131 (2005).
32. M. S. Cosgrove *et al.*, *Biochemistry* **45**, 7511–7521 (2006).
33. S. Han, B. V. Le, H. S. Hajare, R. H. G. Baxter, S. J. Miller, *J. Org. Chem.* **79**, 8550–8556 (2014).

ACKNOWLEDGMENTS

The authors thank N. P. King and P.-S. Huang for helpful discussions. D.B and J.H.M. were supported by the Defense Threat Reduction Agency (HDTRA1-11-1-0041). J.H.M. was supported by National Institute of General Medical Science of the National Institutes of Health under award F32GM099210. P.G.S. acknowledges support by the National Institutes of Health under award 2 R01 GM097206-05. The content is solely the responsibility of the authors and does not represent the official views of the National Institutes of Health. Structures of BIF_1, BIF_1.1 to BIF_1.4, and BIF_0 have been deposited in the Protein Data Bank under accession numbers 4S02, 4S0J, 4S0L, 4S0I, 4S0K, and 4S03.

SUPPLEMENTARY MATERIALS

www.sciencemag.org/content/347/6224/863/suppl/DC1
Materials and Methods
Figs. S1 and S2
Tables S1 and S2
References (*34*–*42*)

6 November 2014; accepted 20 January 2015
10.1126/science.aaa2424

ANIMAL EVOLUTION

Cope's rule in the evolution of marine animals

Noel A. Heim,[1]* Matthew L. Knope,[1]† Ellen K. Schaal,[1]‡ Steve C. Wang,[2] Jonathan L. Payne[1]

Cope's rule proposes that animal lineages evolve toward larger body size over time. To test this hypothesis across all marine animals, we compiled a data set of body sizes for 17,208 genera of marine animals spanning the past 542 million years. Mean biovolume across genera has increased by a factor of 150 since the Cambrian, whereas minimum biovolume has decreased by less than a factor of 10, and maximum biovolume has increased by more than a factor of 100,000. Neutral drift from a small initial value cannot explain this pattern. Instead, most of the size increase reflects differential diversification across classes, indicating that the pattern does not reflect a simple scaling-up of widespread and persistent selection for larger size within populations.

Body size constrains key ecological and physiological traits such as generation time, fecundity, metabolic rate, population size, and home range size (*1*, *2*). Because of perceived advantages associated with larger size, there has long been speculation that animals tend to increase in size over evolutionary time (*3*–*8*), a pattern commonly referred to as Cope's rule. Fossil data support size increase in many cases (*6*, *9*–*15*), but numerous counterexamples also exist (*16*–*22*). Moreover, some instances of size increase could simply result from neutral drift away from an initially small size rather than requiring any active selection for size (*17*, *22*).

To determine whether animal sizes have increased since the start of the Cambrian [542 million

[1]Department of Geological and Environmental Sciences, Stanford University, 450 Serra Mall, Stanford, CA 94305, USA. [2]Department of Mathematics and Statistics, Swarthmore College, Swarthmore, PA 19081, USA.
***Corresponding author. E-mail: naheim@stanford.edu** †Present address: Department of Biology, Stanford University, Stanford, CA 94305, USA. ‡Present address: Department of Geology, Lawrence University, Appleton, WI 54911, USA.